Resources, Conservation & Recycling 161 (2020) 105007

Contents lists available at ScienceDirect

Resources, Conservation & Recycling

journal homepage: www.elsevier.com/locate/resconrec

Full length article

Machine vision estimates the polyester content in recyclable waste textiles

Mikko Mäkelä[a,b,*], Marja Rissanen[a], Herbert Sixta[a]

[a] Aalto University, School of Chemical Engineering, Department of Bioproducts and Biosystems, PO Box 16300, 00076 Aalto, Finland
[b] Swedish University of Agricultural Sciences, Department of Forest Biomaterials and Technology, Skogsmarksgränd, 90183 Umeå, Sweden

ARTICLE INFO

Keywords:
Textiles
Cellulose
Polyester
Hyperspectral imaging
Near infrared
Regression

ABSTRACT

Global textile production is mainly based on polyester and cotton fibers. A majority of textiles at the end of their lifecycle are currently landfilled or incinerated, but will be increasingly recycled in the future. Here, we discuss how the polyester content in blended textiles can be estimated based on hyperspectral near infrared imaging with the aim of developing machine vision for textile characterization and recycling. Differences in the textile samples were first visualized based on a principal component model and the polyester contents of individual image pixels were then predicted using image regression. The results showed average prediction errors of 2.2-4.5% within a range of 0-100% polyester and enabled visualizing the spatial changes in the polyester contents of the textiles. We foresee that digitalized tools similar to what we report here will be increasingly important in the future as more emphasis is placed on coordinated collection, sorting and reuse of waste textiles.

1. Introduction

The need to rethink and redesign the linear textile lifecycle has increased our attention to find new ways to recycle and produce textiles. The average annual growth in the global textile fiber production has been approximately 3% since the 1980's, totaling 107 million tons in 2018 (The Fiber Year, 2019). Polyester and cotton are the most produced fibers, with estimated production volumes of 55 and 26 million tons, respectively (The Fiber Year, 2019). Clothing represents 60% of the global textile consumption and the annual fiber production for consumer clothing has been recently estimated as 53 million tons, of which only 12% are being recycled and 73% end up in landfills or waste incinerators (The Ellen MacArthur Foundation, 2017). Over 97% of the raw materials required for global clothing production are based on virgin feedstock, the majority of which are synthetic fibers (63%) and renewable cotton (26%) (The Ellen MacArthur Foundation, 2017). Pure cotton can be mechanically or chemically recycled and finally respun to produce new yarns at the end of a textile's lifecycle (Haslinger et al., 2019a). Interwoven cotton and polyester blends are however known to be extremely difficult to handle, but remain one of the most prominent mixtures on the clothing market (Haslinger et al., 2019b). Several strategies based on the use of different solvents have thus been recently proposed for separating fibers from mixtures of polyester and other fibers (Haslinger et al., 2019b; Navone et al., 2020; Paunonen et al., 2019; Yousef et al., 2020). Independent of the chosen strategy, quick and reliable methods to accurately determine the polyester content of cotton and polyester blends are urgently needed to enable future large-scale separation and sorting of waste textiles.

A European standard exists for determining the content of virgin or man-made cellulosic and polyester fibers in cotton and polyester mixtures (European Committee for Standardization, 2017). This method is based on concentrated sulfuric acid decomposition of cellulose fibers and gravimetric determination of the remaining extraction residue. The procedure provides a means for accurately determining the chemical composition of cotton and polyester blends under laboratory conditions and has been incorporated in the relevant European Union (EU) regulation on the use of textile labels (European Union Regulation 1007/2011). However, the method is simply too time-consuming and expensive for the analysis of waste textiles for recycling operations. Spectroscopic methods have been proposed as potential alternatives that could be applied even under process conditions. Promising studies on the use of near infrared (NIR) spectroscopy and chemometrics for textile analysis were published already more than two decades ago (Blanco et al., 1994; Cleve et al., 2000; Jasper and Kovacs, 1994; Ruckebusch et al., 2006; Sohn et al., 2005). As an example, different fiber types have been classified (Cleve et al., 2000; Jasper and Kovacs, 1994), and the cotton content of cotton and polyester blends has been predicted after variable selection by genetic algorithms (Ruckebusch et al., 2006). These earlier reports have also been complemented with very recent studies on the use of NIR-based fiber classification (Tan et al., 2019) and quantification (Chen et al., 2019; Liu et al., 2018) and prediction of cellulose and polyester contents in

* Corresponding author at: VTT Technical Research Centre of Finland Ltd., PO Box 1000, 02044 VTT, Finland
E-mail addresses: mikko.makela@vtt.fi, mikko.makela@slu.se (M. Mäkelä).

https://doi.org/10.1016/j.resconrec.2020.105007
Received 6 April 2020; Received in revised form 28 May 2020; Accepted 9 June 2020
Available online 20 June 2020

textile blends using nuclear magnetic resonance (Haslinger et al., 2019c).

Traditional spectrometers measure an average spectrum from one or several arbitrary locations within a sample. For textiles this approach can be sufficient if the sample can be assumed to be homogeneous. In other cases, however, an imaging approach is required. In hyperspectral imaging a full spectrum is recorded in every single pixel of an image combining chemical information with the spatial information of an image. Line-scanning or push-broom instruments record full spectra from a line of pixels as the sample moves under the camera providing an analogy with the identification of objects moving on conveyer belts. It also requires illuminating only one line of pixels at a time, which reduces lighting requirements and increases the speed of image acquisition. Instruments that operate within the NIR region also show increased penetration depths compared with other vibrational techniques (Manley, 2014). This removes the need for laborious sample preparation and makes them extremely appealing alternatives also for recyclable waste textiles.

Hyperspectral NIR images have previously been used for analyzing textile properties. Most of this previous work has focused on using NIR or visible-NIR systems for fiber or foreign object identification (Blanch-Perez-del-Notario et al., 2019; Jin et al., 2017; Li et al., 2019; Zhang et al., 2016), or on predicting the properties of textiles after lamination or finishing procedures (Mirschel et al., 2019; Mirschel et al., 2016, 2017, 2018). Our objective was to determine the potential of hyperspectral NIR cameras in reliably predicting the polyester content of natural and man-made cellulose and polyester blends. Here, we will discuss the calibration of hyperspectral NIR images of textile samples against externally measured polyester contents using image regression, and how the important NIR wavelengths can be identified based on subset selection using interval regression. We believe that these results are important for developing machine vision methods for analyzing textile properties and recycling waste textiles into e.g. new man-made cellulose fibers at the end of the textile lifecycle.

2. Experimental

2.1. Samples and reference analyses

A total of 33 post- and pre-consumer textiles of different colors were used as representative materials for recyclable waste textiles. The sample group contained both “pure” polyester and cotton textiles and their blends, and blends of polyester, recycled cotton, and man-made cellulose fibers, such as viscose and lyocell. Details of individual samples are given in Table S.1 in the Supplementary Information. The samples were first qualitatively analyzed using a light microscope (Leica DMLAM, Leica Microsystems). In general, different textile fibers have characteristic structures which can be identified with a microscope. As illustrated in Fig. S.1, polyester fibers generally have a circular smooth structure whereas cotton fibers have a ribbon-like, twisted structure. Viscose fibers have a serrated structure, which is seen as stripes and lyocell fibers have a circular structure similar to polyester, but show a different texture. Both warp and weft yarns were analyzed separately from woven fabrics and different looking yarns from knitted fabrics. The yarns were unraveled from the fabric, untwisted, and the individual fibers were separated from the end of a yarn and placed on the microscope slide.

After qualitative analysis, the polyester contents of one “pure” polyester and cotton sample and all the fiber blends were determined in duplicate based on acid decomposition according to international standards ISO 1833-1 and ISO 1833-11 (European Committee for Standardization, 2010, 2017) without pretreatment of the samples for removing non-fibrous material. Textile samples of approximately 1 g were first oven-dried at 105 °C overnight and then cooled in a desiccator for at least 2 hours. The cellulose fibers were then dissolved with 75% sulfuric acid at 50 ± 5 °C for 1 hour. The extraction residues were collected in weighted filters and washed with deionized water and diluted ammonia. The residues were then dried at 105 °C overnight, cooled and weighted. The final polyester contents were corrected for moisture as stipulated in the standard. The used correction factors were $a_1 = 8.5$ for cotton, $a_1 = 11.0$ for viscose and lyocell, and $a_2 = 0.4$ for polyester.

2.2. Imaging

Hyperspectral NIR images of the samples with approximate dimensions of 5 × 5 cm were recorded with the same instrument as reported in (Mäkelä et al., 2020). A wavelength range of 1000-2500 nm was chosen as it was not significantly affected by the color of the used textile samples. In short, the images were taken in line-scanning mode where a line of 384 pixels was continuously recorded on different wavelengths. The image field of view was set to approximately 56 mm, which resulted in a nominal pixel size of 150 × 150 μm^2. The images were taken in reflectance mode and converted to absorbance units after correction with external 2, 25, 50, 75 and 99% reflectance target intensities. The targets were evenly spread across the imaged samples and were placed in the same image as one of the samples. The 99% reflectance target was imaged twice, once in the beginning and once in the end of the sample group.

2.3. Image analysis workflow

The reflectance target segments were first separated from the sample images. The sample and the target segments were then median filtered to remove the effects of e.g. dead pixels in the camera detector. Average intensities of 100 target segment rows were used for determining column-wise quadratic regression coefficients based on the average target signals and the externally calibrated reflectance values. The reflectance values from external calibration were interpolated with a second order polynomial to match the wavelengths sampled by the hyperspectral camera. The raw sample images were then converted into reflectance units based on the determined regression coefficients. Overall, this procedure enabled correcting the sample images with the externally calibrated reflectance targets separately for each image column and spectral wavelength. The details of this procedure and its effect on image regression have recently been discussed elsewhere (Mäkelä et al., 2020).

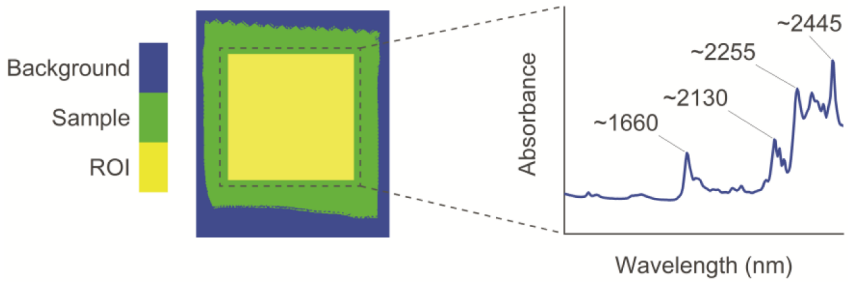

Fig. 1. Image processing. An example of the different image segments with a “pure” polyester sample and the average spectrum of the chosen sample ROI.

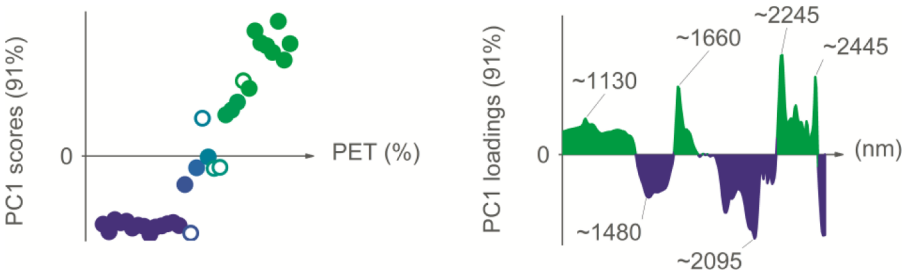

Fig. 2. Exploratory data analysis. Sample scores on the first principal component (left) and the respective loadings (right) based on the average spectra of the samples. The scores were sorted according to increasing polyester (PET) contents in the samples and the unfilled symbols were deemed as outliers and excluded from further image calibration. The numbers in the loadings denote wavelength values in nanometers.

After reflectance calibration the sample images were converted into absorbance for background removal. The image backgrounds were identified and removed using principal components analysis (PCA). Equal-sized regions of interest (ROIs) of 250 × 250 pixels were then selected from the middle of each sample, see Fig. 1. These ROIs were used for exploratory data analysis and image calibration against the externally measured polyester contents of the samples. Exploratory data analysis was first performed based on a PCA (Geladi, 2003) model on one average spectrum per sample according to Eq. (1):

$$\mathbf{Z} = \sum_{i=1}^{n} \mathbf{t_i p_i^T} + \mathbf{E_n} \quad (1)$$

where **Z** denotes a standard normal variate (SNV) (Barnes et al., 1989) transformed and mean centered data matrix of the average spectra of the sample ROIs, $\mathbf{t_i}$ and $\mathbf{p_i}$ the sample scores and orthonormal variable loadings and $\mathbf{E_n}$ a residual matrix after *n* retained principal components (PCs). Fig. 1 illustrates an example of the different image segments and an average sample ROI spectrum.

Image calibration for the respective polyester contents was performed using a partial least squares (PLS) (Martens and Næs, 1989) calibration model. The samples were first divided into separate calibration and test sets by assigning every third sample to the test group. Four average spectra were then extracted from each sample and preprocessed using SNV transformation and mean centering. The polyester contents were also mean centered. The general regression equation between average image spectra and the determined polyester contents can be written as in Eq. (2):

$$\mathbf{y} = \mathbf{Xb} + \mathbf{e} \quad (2)$$

where **y** denotes a vector of measured sample polyester contents, **X** a matrix of average sample spectra, **b** the regression vector and **e** a vector of model residuals. The model vector **b** in Eq. (2) was determined based on the SIMPLS algorithm (de Jong, 1993). Model complexity and the number of latent variables in the PLS model was evaluated based on average prediction errors. These were calculated as the root mean squared errors (RMSE) of calibration (RMSEC) and prediction based on the test set average spectra (RMSEP) and test set image pixel spectra ($RMSEP_{im}$) (Gowen et al., 2014) according to Eq. 3:

$$RMSE = \sqrt{\frac{\sum_{i=1}^{j} (y_i - \hat{y}_i)^2}{j}} \quad (3)$$

where y and $\hat{y}$ denote the measured and predicted polyester contents, respectively, and *j* the number of predicted objects. Image processing and data analysis procedures were based on in-house Matlab® (Version R2018b, The MathWorks, Inc.) routines that partly utilized commercial functions from the PLS Toolbox (Version 8.8, Eigenvector Research, Inc.). The results were plotted in OriginPro (2019, OriginLab Corp.).

3. Results and discussion

3.1. Technical feasibility

Microscopic inspection confirmed that the fibers in the samples matched the ones reported in the textile labels. The polyester contents of all of the textile blends and one "pure" polyester and cotton sample were then determined based on the standard method. The results are given in Table S.2. The pooled standard deviation of the duplicate analyses was 0.29% of moisture-corrected polyester with a respective standard error of 0.21% (n = 2). The deviation between the measured mean polyester contents and the ones reported in the labels across the 14 analyzed samples was on average 1.8% polyester. This average deviation in respect to the two pure samples was 0.35% polyester. As the non-fibrous material was not removed from the fabrics before the analysis, the extraction residues also contained dyes and finishing chemicals which were not soluble in sulfuric acid. Although we were able to analyze only two pure samples, the obtained results and the microscopic evaluation made it possible to assume that the polyester content of the remaining pure samples could be estimated as the content given in the labels. These estimates and the determined mean concentrations were used as reference values for image calibration.

Differences between the individual sample images were first determined using PCA based on one average spectrum per sample ROI after reflectance calibration and image segmentation. PCA is an exploratory data compression method, which decomposes the sample spectra into a set of scores and loadings. The scores describe differences between the samples projected on a set of orthogonal and non-correlated principal components (PCs) and the loadings illustrate their chemical differences based on the changes in the spectra. As illustrated in Fig. 2, the first PC explained 91% of the variation in the preprocessed average spectra and provided a useful separation of the samples based on their polyester contents. The sample scores increased in order of increasing polyester content while ignoring a few exceptions. In PCA, positive sample scores have a positive correlation with positive loadings values, which indicated that the samples with higher polyester contents showed increased absorbance especially at approximately 1130, 1665, 2250 and 2445 nm (Fig. 2). These wavelengths are generally associated with C-H stretching vibrations of aliphatic hydrocarbons and their first and second overtones (Engelsen, 2016; Ruckebusch et al., 2006), and could also be distinguished in the pure polyester spectrum shown in Fig. 1. The samples with low negative loadings showed increased absorbance at approximately 1480 and 2095 nm, which correspond with the stretching vibrations of O-H groups and their first overtones generally seen in e.g. glucose monomers (Osborne et al., 1993; Schwanninger et al., 2011), the building blocks of cellulose chains in cotton or other cellulose-based fibers.

The samples shown with unfilled symbols in Fig. 2 were not in line with the respective polyester contents and showed high standardized residuals during subsequent image regression. Three of these five samples were layered fabrics where most of the other chemical component was situated on one side of the fabric. This suggested that the light measured by the camera detector did not fully penetrate these textiles generating a considerable difference between the predicted and externally measured values. The remaining two samples were white textiles with a glossy surface. We hypothesize that the surface properties of these samples increased their reflectance, which led to underestimating their polyester content by approximately 10 percentage points through the model predictions. These white textiles represented raw fabrics prior to textile dyeing and were made of filament fibers

without delustrants and hence did not represent a typical textile waste flow. Overall, aforementioned five samples were deemed as outliers and were excluded from further image calibration.

After PCA the measured or estimated polyester contents of the samples were regressed on average image spectra using PLS. Four mean spectra were first extracted from each sample ROI and preprocessed using SNV transformation and mean centering. The effects of preprocessing on the raw calibration spectra are illustrated in Fig. S.2. The PLS SIMPLS algorithm determines a latent variable calibration model from the cross-product of both the **X** and the **y** blocks, see Eq. (2), thus taking into consideration the covariance between the calibration spectra and the measured sample properties. The use of latent variables enables having more spectral variables than sample objects, which is a common situation in spectral calibration. Like PCA, the final model predictions can also be presented as combination of scores and loadings and thus depend on how many latent variables are finally used. The initial calibration results are illustrated in Fig. 3. The average prediction errors determined using the mean calibration and test set spectra suggested that three or five latent variables would be appropriate. However, the pooled RMSE values of individual test set image pixels showed that model accuracy did not improve after two latent variables. These results indicated that relying solely on prediction errors determined through average ROI spectra easily led to image overfitting. As our objective was to obtain accurate image predictions, prediction errors based on individual test set pixel spectra were an obvious choice and suggested the use of two latent variables.

However, the entire wavelength range was used for initial image calibration and not all wavelength variables are necessarily equally important for a regression model. In multivariate calibration, potential outliers in the object dimension are generally identified through different diagnostic tools such as model residuals or normalized prediction errors. The aim is to improve overall model quality by removing these outliers. This analogy can also be applied in the wavelength dimension by using variable selection with the aim of excluding unnecessary and potentially noisy wavelengths and thereby enhancing the quality of model predictions. Many different methods exist (Andersen and Bro, 2010; Mehmood et al., 2012), some of which rely on internal model parameters or incomplete or stochastic procedures for selecting the wavelengths. We used a variable selection procedure which combined interval PLS and subset selection. Subset or best subset selection is well-known in multiple linear regression and generally determines model performance based on all possible combinations of individual predictors (Andersen and Bro, 2010). It requires testing a large number models and is prone to over-fitting (Babyak, 2004; Roecker, 1991). Using individual wavelength variables however makes no sense in hyperspectral image regression as the neighboring spectral variables typically show a degree of collinearity and the sampling frequency of the variables can be higher than the reported spectral resolution of the instrument.

Thus, the spectral range was divided into 14 equal-sized intervals and the performance of the calibration model in predicting the test set objects was determined for all possible combinations when 14 to 1 intervals were used. This amounted to using an interval size of 19 spectral variables and calculating a total of 16,383 models. The results are presented not as the lowest absolute prediction errors attainable with a specific number of intervals, but as the relative occurrence of an interval in the model quartile with the lowest RMSEP. Relative occurrence was defined as the number of times a specific interval occurred in the model quartile with the lowest RMSEP divided by the total number of models in that quartile. As illustrated in Fig. 4A, this relative occurrence decreased with the number of used intervals simply because there were more available interval combinations. However, focusing on interval occurrence enabled identifying the intervals that steadily performed well in predicting the average concentrations of the test set samples. This approach was chosen as the differences in the lowest RMSEP values attainable with the best combinations were so small that they were hardly distinguishable considering the standard error of 0.21% polyester obtained from the standard acid decomposition method. The lowest RMSEP values as a function of the number of intervals used and the interval designations are further shown in Fig. S.3.

Intervals numbered 5, 6, 7, 10 and 12 in Fig. 4A were used for final model calibration and the respective average prediction errors are illustrated in Fig. 4B. The results showed that an additional latent variable was required for minimizing RMSEP and $RMSEP_{im}$ after the variable selection procedure. As illustrated in Table 1, the average prediction errors decreased from 3.5-6.6% obtained during initial model calibration with two latent variables to 2.2-4.5% polyester based on variable selection and three latent variables according to the test set average spectra and pixel populations. Variable selection also made it easier to estimate the correct number of latent variables required for the final model as shown by the distinct minimum in the $RMSEP_{im}$ value based on the test set image pixels on three latent variables shown in Fig. 4B. The final model led to an acceptable agreement between the predicted and observed polyester values for the calibration and test objects (Fig. 4C, Table S.3). The model had a remaining test set prediction bias of -1.5% polyester indicating that the predictions were on average slightly lower than the measured or estimated values used for model validation. Especially some of the “pure” polyester samples showed lower predicted values, but these prediction errors were accepted in lack of a more representative sample set and more extensive reference analyses. Increasing the number of samples and the coverage of external polyester determinations would help in correcting these issues in the future.

The obtained absolute average prediction errors after variable selection were comparable or slightly higher than those previously reported for cotton (Blanco et al., 1994; Ruckebusch et al., 2006; Liu et al., 2018) or polyester (Chen et al., 2019) in blends of polyester and other fibers using traditional spectrometers. However, comparing these previous results with the ones reported in this work is not entirely straightforward as hyperspectral cameras generally have a comparably lower spectral resolution but record a significantly higher number of

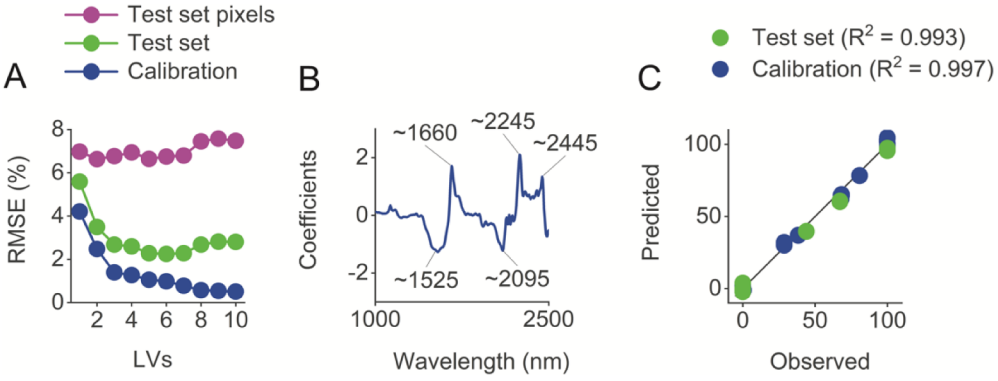

Fig. 3. Initial image calibration. Root mean squared errors (RSME) based on the average calibration and test set spectra and the individual test set pixels as a function of latent variables used in the model (A), the regression vector on 2 latent variables (B) and the predicted vs. observed PET contents (%) based on 2 latent variables (C).

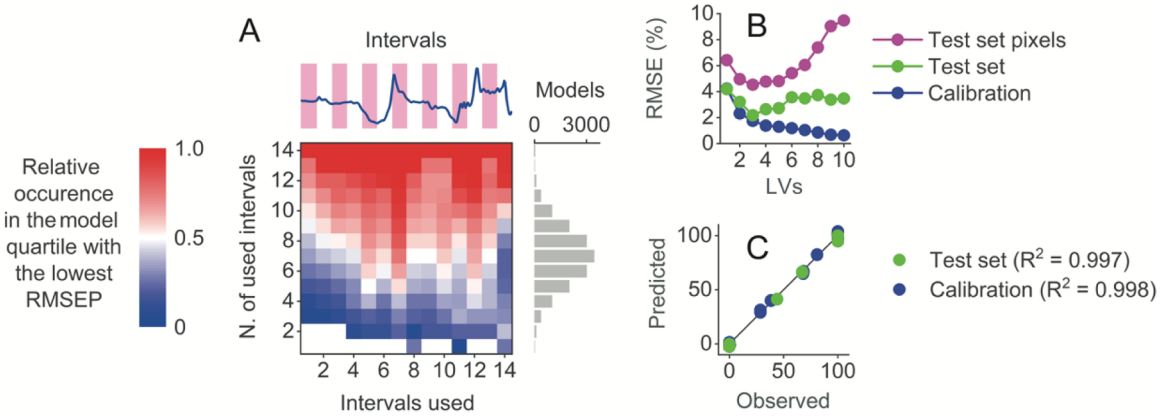

Fig. 4. Variable selection and image calibration. Relative occurrence of individual intervals in the model quartile with the lowest RMSEP during variable selection (A), average prediction errors with intervals 5, 6, 7, 10 and 12 as a function of latent variables (B), and the predicted and observed polyester contents (%) based on three latent variables (C).

spatially assigned pixel spectra in the form of an image. Using cameras instead of point measurements also offers the additional advantage of object identification from mixed material feeds transported on conveyor belts. This is relevant from a practical point of view, as most large-scale textile sorting and recycling facilities in the future will likely operate with a highly heterogeneous textile feed. In addition, it is important to take into account the range and variation of the original refence values when interpreting prediction errors. Different terminologies and methods exist in the literature, but most authors normalize the standard deviation of the reference values with the standard error of prediction (Williams and Sobering, 1993), which is essentially RMSEP corrected for bias (Martens and Næs, 1989). For our results, this ratio of prediction to standard deviation (RPD) was 27, which has been reported to be sufficient for most applications according to the general rules of thumb within the NIR field (Manley, 2014). However, this discussion is provided only as a directional guideline and the results should be interpreted with caution due to the relatively small amount of samples available for model calibration and validation.

Finally, the determined calibration model was used for predicting the polyester contents of individual image pixels to visualize the spatial changes in the chemical composition of the textiles. Examples of these predictions are illustrated in Fig. 5. The model predictions successfully separated the spatial regions with differences in the polyester content within the blended textiles. In addition, samples with visual differences that were composed entirely of polyester showed no distinct differences in the predicted images (Fig. 5). The lyocell and polyester blend in Fig. 5 was in fact made with a jacquard knitting technique (Spencer, 2001). The imaging side the sample thus had distinct and separate spatial regions of lyocell and polyester thread. The other side however showed a scrambled color appearance in which the different chemical regions were not easily distinguishable (Fig. S.4). The polyester regions in the lyocell and polyester blend sample shown in Fig. 5 were thus not composed entirely of polyester throughout the sample cross-section which decreased the predicted values of the polyester pixels from 100% “pure” polyester to approximately 60% as shown in the pixel histogram.

3.2. Environmental and economic aspects

The obtained results showed that the polyester contents of blended textiles can be estimated based on hyperspectral NIR image regression with acceptable reliability. These results are significant as e.g. most chemical recycling strategies can currently cope with only a limited amount of polyester in the recyclable textile material and this share needs to be reliably estimated. In practice, waste textiles could be first classified into different fiber types and the exact chemical composition of polyester and cellulose blends could then be predicted to evaluate whether they could be chemically recycled. From a mathematical point of view this constitutes a straightforward extension of image analysis based on the same image. It is likely that new digitalized tools will soon be required for textile sorting in Europe as EU member states are currently required to separately collect household textile waste by 2025 (European Council, 2018). In the following we will shortly discuss the environmental and economic aspects of textile sorting and utilization in Finland where data were available.

Dahlbo et al. (2017) have recently estimated the environmental impacts of different textile reuse and recycling scenarios in Finland, where it has been forbidden to landfill organic waste including textiles since 2016. The authors evaluated the environmental performance of the scenarios based on the domestic use of textile products in 2012, which was on average 13.2 kg per capita. Approximately 20% of discarded textiles were at that time separately collected for reuse by charity organizations and the remaining 80% ended up in municipal solid waste. The largest improvement in environmental performance was generated by increased reuse of discarded textile waste followed by chemical recycling although the differences between the two were very small. For both scenarios, the improvement in environmental performance was mainly due to avoided primary production. However, only a share of separately collected textile waste can be directly reused and both reuse and recycling will be required in the future.

Heikkilä et al. (2019) also recently estimated the costs of textile recycling to evaluate different recycling alternatives in Finland. Their calculations were based on the same 80% share of domestically used

Table 1
Model performance before and after variable selection.

Model	Wavelength variables	Used wavelengths (nm)	Calibration and test objects	Used LVs	R^2_{cal}, R^2_{test}	RMSEC, RMSEP, $RMSEP_{im}$ (%, PET)
Initial calibration model	268	999-2498	76 and 36	2	0.997, 0.993	2.48, 3.50, 6.63
Final calibration model	95	1435-1749, 1967-2068, 2180-2281	76 and 36	3	0.998, 0.997	1.74, 2.19, 4.53

LVs = latent variables.

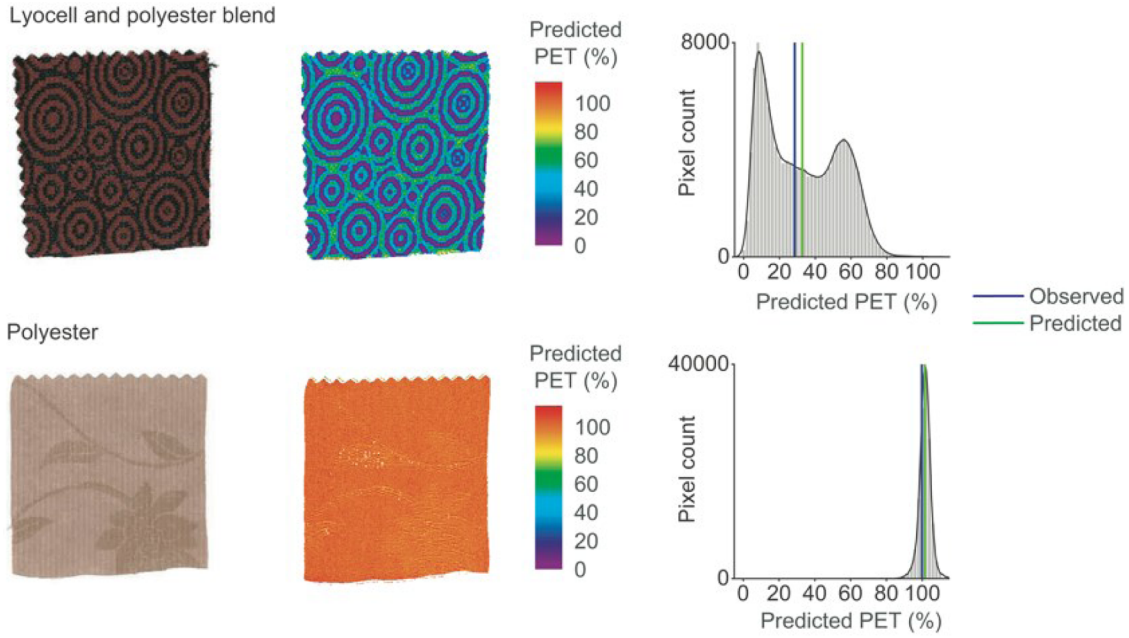

Fig. 5. Image predictions. Two textile samples (left), their polyester contents based on image predictions (middle) and the respective pixel histograms which illustrate the distributions of the predicted pixel values (right). The histograms have different vertical scales and the colored vertical lines denote the mean observed and predicted values. The reader is referred to the electronic version of this article for proper illustration of figure colors.

textiles that ended up in municipal solid waste also used by Dahlbo et al. (2017). The authors found that the total estimated costs of collection and sorting amounted to 0.43 €/kg textile waste. Recycling the actual fibers was more expensive, approximately 0.5-0.6 €/kg and 0.85 €/kg for mechanically and chemically recycled textiles, respectively. The maximum overall costs of approximately 1.3 €/kg of recycled waste textiles was still lower than the world market prices for cotton or polyester (Heikkilä et al., 2019). This implies that the collection, sorting and recycling of waste textiles would be economically feasible. It must be stated, however, that these scenarios still relied on the willingness of consumers to separate their used textiles and the latest digitalized and automated tools for centralized textile sorting.

4. Conclusions

We have illustrated how hyperspectral NIR images can be calibrated for predicting the polyester contents of textiles using image regression. This approach is one alternative for estimating the chemical composition of textile blends in situations where information on the spatial changes in their composition is required. Hyperspectral images are typically calibrated based on the measured average concentrations of an analyte, while the overall aim is to accurately predict individual image pixels where no reference values are available. Based on the obtained results, the average prediction errors in respect to mean test set spectra were 2.2% polyester, while the pooled estimate based on individual test set pixel spectra and average sample concentrations suggested a prediction error of 4.5% within a range of 0-100% polyester. The initial data exploration also showed that there were identifiable uncertainties related to the different layers and surface properties with some of the sampled textiles. These uncertainties created considerable differences between the measured absorbance and externally determined polyester contents of the samples. In this work these samples were excluded as outliers, but future efforts should acknowledge these issues when further developing machine vision for textile characterization. We anticipate that digitalized methods similar to what has been reported here will be increasingly important in the future as more and more emphasis is placed on coordinated collection, sorting and utilization of waste textiles.

CRediT authorship contribution statement

Mikko Mäkelä: Conceptualization, Methodology, Software, Validation, Formal analysis, Investigation, Resources, Data curation, Writing - original draft, Writing - review & editing, Visualization, Project administration, Funding acquisition. **Marja Rissanen:** Conceptualization, Methodology, Formal analysis, Investigation, Resources, Writing - original draft, Writing - review & editing, Visualization, Project administration. **Herbert Sixta:** Conceptualization, Resources, Writing - review & editing, Project administration, Funding acquisition.

Declaration of Competing Interests

The authors declare that they have no known competing financial interests or personal relationships that could have appeared to influence the work reported in this paper.

Acknowledgements

We acknowledge Marja Kärkkäinen from Aalto University for her help in performing the reference analyses. This work was financially supported by the Strategic Research Council of the Academy of Finland under grant agreement no. 327296 - the FINIX project (finix.aalto.fi).

Supplementary materials

Supplementary material associated with this article can be found, in the online version, at doi:10.1016/j.resconrec.2020.105007.

References

Andersen, C.M., Bro, R., 2010. Variable selection in regression - a tutorial. J. Chemometr. 24, 728–737. https://doi.org/10.1002/cem.1360.

Babyak, M.A., 2004. What you see may not be what you get: a brief, nontechnical introduction to overfitting in regression-type models. Psychosom. Med. 66, 411–421. https://doi.org/10.1097/01.psy.0000127692.23278.a9.

Barnes, R.J., Dhanoa, M.S., Lister, S.J., 1989. Standard normal variate transformation and de-trending of near-infrared diffuse reflectance spectra. Appl. Spectrosc. 43, 772–777. https://doi.org/10.1366/0003702894202201.

Blanch-Perez-del-Notario, C., Saeys, W., Lambrechts, A., 2019. Hyperspectral imaging for textile sorting in thge visible-near infrared range. J. Spectr. Imag. 8, a17. https://doi.org/10.1255/jsi.2019.a17.

Blanco, M., Coello, J., Iturriaga, H., Maspoch, S., Bertran, E., 1994. Analysis of cotton-polyester yarns by near-infrared reflectance spectroscopy. Analyst 119, 1779–1785. https://doi.org/10.1039/AN9941901779.

Chen, H., Tan, C., Lin, Q., 2019. Quantitative determination of the fiber components in textiles by near-infrared spectroscopy and extreme machine learning. Anal. Lett. https://doi.org/10.1080/00032719.2019.1683742.

Cleve, E., Bach, E., Schollmeyer, E., 2000. Using chemometric methods and NIR spectrophotometry in the textile industry. Anal. Chim. Acta 420, 163–167. https://doi.org/10.1016/S0003-2670(00)00888-6.

Dahlbo, H., Aalto, K., Eskelinen, H., Salmenperä, H., 2017. Increasing textile circulation - consequences and requirements. Sustain. Prod. Consum. 9, 44–57. https://doi.org/10.1016/j.spc.2016.06.005.

de Jong, S., 1993. SIMPLS: an alternative approach to partial least squares regression. Chemom. Intell. Lab. Syst. 18, 251–263. https://doi.org/10.1016/0169-7439(93)85002-X.

Engelsen, S.B., 2016. Near infrared spectroscopy - a unique window of opportunities. NIR news 27, 14–17. https://doi.org/10.1255/nirn.1620.

European Council, 2018. Waste management and recycling: council adopts new rules, press release. Available at: www.consilium.europa.eu/en/press/press-releases/2018/05/22/waste-management-and-recycling-council-adopts-new-rules/ [accessed April 6th, 2020].

The Ellen MacArthur Foundation, 2017. A new textiles economy: Redesigning fashion's future. Available at: www.ellenmacarthurfoundation.org/publications/a-new-textiles-economy-redesigning-fashions-future [accessed April 3rd, 2020].

European Committee for Standardization (2010). Textiles - quantitative chemical analysis - part 1: general principles of testing (ISO-1833-11:2006, including cor 1:2009).

European Committee for Standardization (2017). Textiles - quantitative chemical analysis - part 11: mixtures of certain cellulose fibres with certain other fibres (method using sulfuric acid) (ISO-1833-11:2017).

European Union Regulation 1007/2011. Regulation (EU) No 1007/2011 of the European parliament and of the council of 27 september 2011 on textile fibre names and related labelling and marking of the fibre composition of textile products and repealing council directive 73/44/EEC and directives 96/73/EC of the European parliament and of the council (2011). Available at: eur-lex.europa.eu [accessed April 3rd, 2020].

Geladi, P., 2003. Chemometrics in spectroscopy. Part 1. Classical chemometrics. Spectroc. Acta, Part B 58, 767–782. https://doi.org/10.1016/S0584-8547(03)00037-5.

The Fiber Year GmbH, 2019. The fiber year 2019 - the survey on textiles & nonwovens. Available at: https://thefiberyear.com/home/ [accessed April 3rd, 2020].

Gowen, A., Burger, J., Esquerre, C., Downey, G., O'Donell, C., 2014. Near infrared hyperspectral image regression: on the use of prediction maps as a tool for detecting model overfitting. J. Near Infrared Spectrosc. 22, 261–270. https://doi.org/10.1255/jnirs.1114.

Haslinger, S., Wang, Y., Rissanen, M., Lossa, M.B., Tanttu, M., Ilen, E., Määttänen, M., Harlin, A., Hummel, M., Sixta, H., 2019a. Recycling of vat and reactive dyed textile waste to new colored man-made cellulose fibers. Green Chem. 21, 5598–5610. https://doi.org/10.1039/c9gc02776a.

Haslinger, S., Hummel, M., Anghelescu-Hakala, A., Määttänen, M., Sixta, H., 2019b. Upcycling of cotton polyester blended textile waste to new man-made cellulose fibers. Waste Manage 97, 88–96. https://doi.org/10.1016/j.wasman.2019.07.040.

Haslinger, S., Hietala, S., Hummel, M., Maunu, S.L., Sixta, H., 2019c. Solid-state NMR method for the quantification of cellulose and polyester in textile blends. Carbohydr. Polym. 207, 11–16. https://doi.org/10.1016/j.carbpol.2018.11.052.

Heikkilä, P. (Ed.), Cura, K., Heikkilä, J., Hinkka, V., Ikonen, T., Kamppuri, T., Knuutila, H., Kokko, M., Lankiniemi, S., Lehtinen, L., Mäkiö, I., Pitkänen, M. (Ed.), Saarimäki, E., Virta, M., Zitting, J., Harlin, A., 2019. Telaketju: towards circularity of textiles. VTT technical research centre of Finland. VTT research report, No. VTT-R-00062-19. Available at: cris.vtt.fi/en/publications/telaketju-towards-circularity-of-textiles [accessed April 6th, 2020].

Jasper, W.J., Kovacs, E.T., 1994. Using neural networks and NIR spectrophotometry to identify fibers. Text. Res. J. 64, 444–448. https://doi.org/10.1177/004051759406400803.

Jin, X., Memon, H., Tian, W., Yin, Q., Zhan, X., Zhu, C., 2017. Spectral characterization and discrimination of synthetic fibers with near-infrared hyperspectral imaging system. Appl. Optics 56, 3570–3576. https://doi.org/10.1364/AO.56.003570.

Li, J., Meng, X., Wang, W., Xin, B., 2019. A novel hyperspectral imaging and modeling method for the component identification of woven fabrics. Text. Res. J. 89, 3752–3767. https://doi.org/10.1177/0040517518821907.

Liu, Y., Zhou, S., Liu, W., Yang, X., Luo, J., 2018. Least-squares support vector machine and successive projection algorithm for quantitative analysis of cotton-polyester textile by near infrared spectroscopy. J. Near Infrared Spectrosc. 26, 34–43. https://doi.org/10.1177/0967033518757069.

Mäkelä, M., Geladi, P., Rissanen, M., Rautkari, L., Dahl, O., 2020. Hyperspectral near infrared image calibration and regression. Anal. Chim. Acta. 1105, 56–63. https://doi.org/10.1016/j.aca.2020.01.019.

Manley, M., 2014. Near-infrared spectroscopy and hyperspectral imaging: non-destructive analysis of biological materials. Chem. Soc. Rev. 43, 8200–8214. https://doi.org/10.1039/c4cs00062e.

Martens, H., Næs, T., 1989. Multivariate Calibration. John Wiley & Sons Ltd, New York.

Mehmood, T., Liland, K.H., Snipen, L., Sæbo, S., 2012. A review of variable selection methods in partial least squares regression. Chemometrics Intell. Lab. Syst. 118, 62–69. https://doi.org/10.1016/j.chemolab.2012.07.010.

Mirschel, G., Daikos, O., Scherzer, T., 2019. In-line monitoring of the thickness distribution of adhesive layers in black textile laminates by hyperspectral imaging. Comput. Chem. Eng. 124, 317–325. https://doi.org/10.1016/j.compchemeng.2019.01.015.

Mirschel, G., Daikos, O., Scherzer, T., Steckert, C., 2016. Near-infrared chemical imaging used for in-line analysis of inside adhesive layers in textile laminates. Anal. Chim. Acta 932, 69–79. https://doi.org/10.1016/j.aca.2016.05.015.

Mirschel, G., Daikos, O., Scherzer, T., Steckert, C., 2017. Near-infrared hyperspectral imaging of lamination and finishing processes in textile technology. NIR news 28, 20–25. https://doi.org/10.1177/0960336016687949.

Mirschel, G., Daikos, O., Scherzer, T., Steckert, C., 2018. Near-infrared chemical imaging used for in-line analysis of functional finishes on textiles. Talanta 188, 91–98. https://doi.org/10.1016/j.talanta.2018.05.050.

Navone, L., Moffitt, K., Hansen, K.-A., Blinco, J., Payne, A., Speight, R., 2020. Closing the textile loop: enzymatic fibre separation and recycling of wood/polyester fabric blends. Waste Manage 102, 149–160. https://doi.org/10.1016/j,wasman.2019.10.026.

Osborne, B.G., Fearn, R., Hindle, P.H., 1993. Practical NIR Spectroscopy with applications in Food and Beverage Analysis, 2nd ed. Pearson Education Limited, United Kingdom.

Paunonen, S., Kamppuri, T., Katajainen, L., Hohenthal, C., Heikkilä, P., Harlin, A., 2019. Environmental impact of cellulose carbamate fibers from chemically recycled cotton. J. Clean. Prod. 222, 871–881. https://doi.org/10.1016/j.clepro.2019.03.063.

Roecker, E.B., 1991. Prediction error and its estimation for subset-selected models. Technometrics 33, 459–468. https://doi.org/10.1080/00401706.1991.10484873.

Ruckebusch, C., Orhan, F., Durand, A., Boubellouta, T., Huvenne, J.P., 2006. Quantitative analysis cotton-polyester textile blends from near-infrared spectra. Appl. Spectrosc. 60, 539–544. https://doi.org/10.1366/000370206777412194.

Schwanninger, M., Rodriques, J.C., Fackler, K., 2011. A review of band assignments in near infrared spectra of wood and wood components. J. Near Infrared Spectrosc. 19, 287–308. https://doi.org/10.1255/jnirs.955.

Sohn, M., Himmelbasch, D.S., Akin, D.E., Barton II, E.F., 2005. Fourier transform near-infrared spectroscopy for determining linen content in linen/cotton blend products. Text. Res. J. 75, 583–590. https://doi.org/10.1177/0040517505057167.

Spencer, D.J., 2001. Knitting technology, 3rd ed. Woodhead Publishing Ltd., Cambridge.

Tan, C., Chen, H., Lin, Z., Wu, T., 2019. Category identification of textile fibers based on near-infrared spectroscopy combined with data description algorithms. Vib. Spectrosc. 100, 71–78. https://doi.org/10.1016/j.vibspec.2018.11.004.

Williams, P.C., Sobering, D.C., 1993. Comparison of commercial near infrared transmittance and reflectance instruments for analysis of whole grains and seeds. J. Near Infrared Spectrosc. 1, 25–32. https://doi.org/10.1255/jnirs.3.

Yousef, S., Tatariants, M., Tichonovas, M., Kliucininkas, L., Lukošiūtė, S.-I., Yan, L., 2020. Sustainable green technology for recovery of cotton fibers and polyester from textile waste. J. Clean. Prod. 254, 120078. https://doi.org/10.1016/j.jclepro.2020.120078.

Zhang, R., Li, C., Zhang, M., Rodgers, J., 2016. Shortwave infrared hyperspectral reflectance imaging for cotton foreign matter classification. Comp. Electron. Agric. 127, 260–270. https://doi.org/10.1016/j.compag.2016.06.023.